A molecular switch in RCK2 triggers sodium-dependent activation of K_{Na}1.1 (KCNT1) potassium channels

Bethan A. Cole,[1,5] Antreas C. Kalli,[2,3] Nadia Pilati,[4] Stephen P. Muench,[1,3] and Jonathan D. Lippiat[1,*]

[1]School of Biomedical Sciences, University of Leeds, Leeds LS2 9JT, UK.

[2]Leeds Institute of Cardiovascular and Metabolic Medicine, University of Leeds, Leeds LS2 9JT, UK.

[3]Astbury Centre for Structural and Molecular Biology, University of Leeds, Leeds LS2 9JT, UK.

[4]Autifony Srl, Padova, 35127, Italy.

[5]Present address: Nuffield Department of Clinical Neurosciences, University of Oxford, Oxford OX3 9DU, UK.

*Correspondence: j.d.lippiat@leeds.ac.uk

Running title: A molecular switch in K_{Na} channels

Abstract

The Na^+-activated K^+ channel $K_{Na}1.1$, encoded by the *KCNT1* gene, is an important regulator of neuronal excitability. How intracellular Na^+ ions bind and increase channel activity is not well understood. Analysis of $K_{Na}1.1$ channel structures indicate that there is a large twisting of the βN-αQ loop in the intracellular RCK2 domain between the inactive and Na^+-activated conformations, with a lysine (K885, human subunit numbering) close enough to potentially form a salt bridge with an aspartate (D839) in βL in the Na^+-activated state. Concurrently, an aspartate (D884) adjacent in the same loop adopts a position within a pocket formed by the βO strand. In carrying out mutagenesis and electrophysiology with human $K_{Na}1.1$, we found alanine substitution of selected residues in these regions resulted in almost negligible currents in the presence of up to 40 mM intracellular Na^+. The exception was D884A, which resulted in constitutively active channels in both the presence and absence of intracellular Na^+. Further mutagenesis of this site revealed an amino acid size-dependent effect. Substitutions at this site by an amino acid smaller than aspartate (D884V) also yielded constitutively active $K_{Na}1.1$, D884I had Na^+-dependence similar to wild-type $K_{Na}1.1$, whilst increasing the side chain size larger than aspartate (D884E or D884F) yielded channels that could not be activated by up to 40 mM intracellular Na^+. We conclude that Na^+ binding results in a conformational change that accommodates D884 in the βO pocket, which triggers further conformational changes in the RCK domains and channel activation.

Statement of Significance

Sodium-activated potassium channels regulate neuronal excitability, and their dysfunction causes severe childhood disorders. Here, we identify a structural determinant in the intracellular domains that is responsible for triggering channel activation in response to sodium ion binding. An increase in the size of a particular amino acid renders the channel sodium-insensitive, whilst a decrease in size enables the channel to activate in the absence of sodium. This enhances our understanding of how this subclass of potassium channels respond to changes in the intracellular ionic environment. Furthermore, this may also further our understanding of the basis of human neurological disorders and their treatment.

Introduction

Na^+-activated K^+ channels (K_{Na}) open in response to elevation in the cytoplasmic Na^+ concentration, contributing to hyperpolarization of the membrane potential of neurons and other cell types. $K_{Na}1.1$ and $K_{Na}1.2$ (or SLACK and SLICK) are members of the large-conductance, RCK domain-containing subfamily of K^+ channels and are activated by intracellular Na^+ (1). Intracellular Na^+ is an essential determinant of wild-type (WT) $K_{Na}1.1$ channel opening, and in normal physiology $K_{Na}1.1$ activity is coupled to persistent inward Na^+ currents, for example through re-opening voltage-gated Na^+ channels or NALCN channels that increase local Na^+ concentration above that of the bulk cytosol (2, 3). Additionally, transient currents through AMPA receptors located in the vicinity of $K_{Na}1.1$ have also been implicated as a Na^+ source for the channel, as part of a negative-feedback loop (4). The importance of these channels is highlighted by the seizure disorders and intellectual disability caused by pathogenic variants in either K_{Na}-encoding gene, *KCNT1* or *KCNT2* (5-9). In most cases, pathogenic variants in either gene result in a missense mutation that leads to enhanced K_{Na} channel activity, but loss of function is also found with some *KCNT2* variants (10). Quinidine, bepridil, and clofilium were the first drugs to be identified as K_{Na} channel inhibitors with bithionol, riluzone, loxapine, and niclosamide as activators (11-13). Each of these drugs are non-selective and are unlikely to be of clinical use in K_{Na} disorders. In response to *KCNT1* gain-of-function disorders, several groups have identified novel $K_{Na}1.1$ channel inhibitors (14-16). Our approach exploited K_{Na} channels structures and targeted the pore domain in virtual high throughput screening (14), but it is conceivable that future structure-based screening could instead target the Na^+-activation mechanism, which could improve specificity. However, the structural basis of how Na^+ ions interact with K_{Na} channels and how this results in channel activation remains unknown.

Previously, residues located in the rat $K_{Na}1.1$ RCK2 domain were proposed to form a Na^+ binding site based upon a Na^+ coordination motif, DXRXXH that is found in Na^+-activated GIRK channels (17). Mutating D818 and, to a lesser degree, H823 diminished rat $K_{Na}1.1$ Na^+-activation when the channels were expressed and recorded from patches excised from *Xenopus* ooctyes. In general, Na^+ sensitivity was shifted to higher concentrations for channels mutated at either site (17). In human $K_{Na}1.2$, mutation of the equivalent aspartate residue, D757, to arginine abolished Na^+-activation in whole *Xenopus* oocytes, with function rescued by application of the activator niflumic acid (18). The structures of the chicken $K_{Na}1.1$ channel in the closed (zero Na^+ conditions) and activated (high Na^+ conditions)

conformations were since resolved by cryogenic electron microscopy (cryo-EM) and single particle averaging (19, 20), in which the Na^+-binding fold proposed by Zhang and others (17) was not evident. The region containing the proposed DXRXXH coordination motif is conserved between chicken and rat $K_{Na}1.1$ but remains as a static loop in both the active and inactive conformations, as will be described below. Since Na^+ ions, owing to their size, are usually unresolved in structures generated by cryo-EM, it is not known where in the channel they bind and how this results in increased channel activity.

In studying the cryo-EM structures of the inactive and active chicken $K_{Na}1.1$ channel subunits, we identified a conformational difference between the two that we hypothesized could underlie Na^+-dependent activation. Furthermore, it appeared to involve the aspartate residue identified by Zhang and others (17) in playing a conformation-stabilizing role. Using site-directed mutagenesis and electrophysiology we identify additional residues in a nearby region that are critical for Na^+-dependent activation and propose that a twisting of a loop between βN and αQ in RCK2 acts as a molecular switch that underlies $K_{Na}1.1$ activation. Whilst preparing this manuscript, complementary studies on $K_{Na}1.1$ Na^+-binding and activation were published, involving molecular dynamics simulations and mutagenesis (21) or cryo-EM (22), together with functional characterization. In presenting and discussing our findings we highlight where our interpretation is consistent or conflicts with the conclusions of either of these studies.

Materials and Methods

Analysis of protein structures

Structures of chicken $K_{Na}1.1$ in the Na^+-activated (PDB: 5U70) and Na^+-free (PDB: 5U76) states (20) were analyzed and figures prepared using UCSF Chimera (23). Amino acid substitutions were introduced *in silico* using the Rotamer function and assessed using the Find Clashes/Contacts function. Initially, the rotamer with the highest probability, with respect to the chi parameters generated from the integrated Dunbrack 2010 library was selected. If intramodel atomic clashes were obtained, the next two rotamers in the probability ranking were evaluated. Molecular surfaces were calculated using the MSMS tool within Chimera (24).

Molecular biology and transfection

The full-length pcDNA6-K_{Na}1.1 mammalian expression plasmid that we described previously (14) was used in these studies. Mutations were designed and introduced by polymerase chain reaction using the New England BioLabs method and confirmed by sequencing (Genewiz, Takeley, U.K.). Due to the large size and high GC content of the insert, mutations were generated in a plasmid containing the SbfI/BsiWI restriction fragment, and then subcloned into the corresponding sites in the pcDNA6-K_{Na}1.1 construct. Chinese hamster ovary (CHO) cells were cultured in Dulbecco's Modified Eagle's Medium (DMEM) (Gibco, Paisley, UK) supplemented with 10 % (v/v) Fetal Bovine Serum (FBS), 50 U/ml penicillin and 0.05 mg/ml streptomycin and incubated at 37°C in 5% CO_2. Cells were co-transfected with WT or mutated pcDNA6-K_{Na}1.1 together with pEYFP-N1 plasmid using Mirus TransIT-X2 reagent (Geneflow, Lichfield, U.K.). For electrophysiological experiments, cells were plated onto borosilicate glass cover slips and used 2-4 days later.

Electrophysiology

All chemicals were obtained from Sigma-Aldrich (Gillingham, U.K.) unless stated otherwise. Micropipettes were pulled from thin-walled borosilicate glass (Harvard Apparatus Ltd, Kent, UK), polished, and gave resistances of 1.5 to 2.5 MΩ in the experimental solutions. The bath (extracellular) solution contained, in mM, 140 NaCl, 1 $CaCl_2$, 5 KCl, 29 Glucose, 10 HEPES and 1 $MgCl_2$, pH 7.4 with NaOH. The 40 mM Na^+ pipette (intracellular) solution contained, in mM, 130 K-Gluconate, 30 NaCl, 29 Glucose, 5 EGTA and 10 HEPES, pH 7.3 with KOH. To obtain pipette solutions containing Na^+ at 10 mM and 0 mM (nominally Na^+-free), the NaCl was replaced by equimolar amounts of choline chloride. K_{Na}1.1 activators loxapine succinate and niclosamide were prepared as 10 mM stock solutions in DMSO. The final drug concentrations were obtained by diluting the stock solution in the bath solution on the day of the experiment.

Currents were recorded from EYFP-fluorescing cells at room temperature (20 to 22°C) in the whole-cell patch clamp configuration using an EPC10 amplifier (HEKA Electronics, Lambrecht, Germany), with >70 % series resistance compensation (where appropriate), 2.9 kHz low-pass filtering, and 10 kHz digitization. Following the establishment of the whole cell configuration, cells were held at -80 mV and 400 ms voltage pulses from -100 to +80 mV in 10 mV increments were applied. With experiments that examine the effect of pharmacological activation, the 10 mM NaCl pipette solution was used, and the voltage

protocol was applied both before and after bath perfusion of 30 μM of either niclosamide or loxapine.

Data analysis

Samples were not randomized and the experiments were not blinded. Data are presented as mean ± SEM from n number of cells. Statistical analysis was performed using SPSS (IBM Analytics, Portsmouth, U.K.), with the chosen tests indicated in figure legends; $p<0.05$ was considered significant. Without *a priori* knowledge of effect sizes, power calculations were not conducted. Representative whole-cell current traces were plotted, and residual capacitance spikes removed in OriginPro. Whole-cell current-voltage relationships were divided by whole-cell capacitance to give current density (pA/pF). Reversal potentials were obtained by fitting the linear part of current-voltage relationships around the reversal potential using linear regression and determining the voltage at the zero current level. Conductance values (G) at each voltage (V_m) were obtained by dividing current amplitudes (I) by the driving force on K^+ ions, calculated using the reversal potentials (V_{rev}) obtained in individual recordings: $G=I/(V_m-V_{rev})$. The conductance values were plotted against V_m and fitted with a Boltzmann function, $G=(G_{max}-G_{min})/(1+e^{(V_m-V_{0.5})/k})+G_{min}$, which gave values for activation midpoint ($V_{0.5}$), G_{max}, G_{min}, and Slope factor (k). Data were normalized by dividing by G_{max} for each experiment. Reported $V_{0.5}$ values were corrected for liquid junction potential error after the experiment. With $k = RT/zF$, the valence of the gating charge, z, was estimated.

Results

Identification of a putative Na^+ binding site in $K_{Na}1.1$ structural data

The aspartate residue found by Zhang and others (17) to be critical for Na^+ activation in rat $K_{Na}1.1$, D818, is the equivalent to D812 in chicken and D839 in human $K_{Na}1.1$. To assist comparisons between studies of $K_{Na}1.1$ clones from different species the positions of the amino acids detailed in this study in human, rat, and chicken are provided in Table S1 in the Supporting Material. We hereon refer only to the amino acid numbering in human $K_{Na}1.1$. The proposed Na^+-coordinating motif, based on that in GIRK channels, is conserved between species and forms the loop between βL and αO in the $K_{Na}1.1$ RCK2 domain. Firstly,

the Na^+-binding fold proposed by the molecular modelling and simulations of RCK2 of the rat $K_{Na}1.1$ (17) subunit was not observed in the cryo-EM structures of either the active (PDB: 5U70, Figure 1A) or inactive (PDB: 5U76) chicken $K_{Na}1.1$ channels. Secondly, there was no discernible difference between the two structures in the positioning of the sidechain of this aspartate or any of the neighboring residues previously proposed to contribute to Na^+-binding (D839 in Figure 1B). Notably, in the structure of the Na^+-activated state, a lysine reside in the loop between βN-αQ (K885 in Figure 1B) falls within 3.4 Å of the aspartate, sufficiently close to form a salt bridge. In the apo state this loop is not fully resolved, indicating disorder, but comparison with the structure of the activated state suggests that upon activation by sodium there is a rotation of this loop around the axis of the backbone by approximately 180°. This was observed by Zhang and others (22) to be the case in the structures of human $K_{Na}1.1$. Consequentially, the adjacent aspartate in the same βN-αQ loop (D884 in Figure 1B) adopts a position within a pocket formed by the βO beta strand in RCK2 (Figure 1B). Specifically, the aspartate side chain occupies a crevice between the β-carbons of E920 and T922 sidechains and the L921 backbone. The differences between the cryo-EM structures of chicken $K_{Na}1.1$ in the inactive and Na^+-activated states therefore indicate that the rotation and stabilization of the βN-αQ loop is a conformational change in RCK2 upon Na^+ binding.

Activation of WT $K_{Na}1.1$ by intracellular Na^+ and pharmacological activators

Guided by $K_{Na}1.1$ channel structural data, a combination of mutagenesis and whole-cell electrophysiology was used to investigate the involvement of residues in Na^+-dependent activation of the human $K_{Na}1.1$ channel. In our hands, human $K_{Na}1.1$ runs down within seconds in excised inside-out patches, leaving unitary or no currents. Therefore, to efficiently explore the effects on macroscopic $K_{Na}1.1$ currents, we conducted whole-cell patch clamp recordings from CHO cells expressing WT or mutant $K_{Na}1.1$ using pipette solutions with different concentrations of Na^+ and using pharmacological activation to bypass Na^+-activation and confirm the presence of relatively Na^+-insensitive channels. The anti-psychotic drug loxapine and anti-helminthic drug niclosamide are potent activators of WT $K_{Na}1.1$ with EC_{50} values of 4.4 μM and 2.9 μM, respectively (13). Both drugs also reduce the voltage-dependence of $K_{Na}1.1$ activation, resulting in near-linear current-voltage relationships and increased inward current at voltages negative to the reversal potential (Figure S1). Initially, niclosamide was selected to confirm function expression of “inactive” mutant channels. CHO cells are believed to have little or no endogenous ion conductance (25). However, when 30

μM niclosamide was perfused into the bath a current with density 58.96 ± 9.60 pA/pF at +10 mV was recorded from non-transfected CHO cells, compared to 1.49 ± 0.67 pA/pF at +10 mV prior to its application (n=4 and 5 cells, respectively). Though this current is relatively small in comparison to exogenous $K_{Na}1.1$ current (Figure S1A, B), this could confound the functional rescue of seemingly inactive $K_{Na}1.1$ channels. The identity of the conductance and charge-carrier evoked by niclosamide is unknown, but experiments ruled out $K_{Na}1.1$, since the current was not inhibited by 10 μM bepridil (Figure S1C). The reversal potential (-73.30 ± 0.85 mV, n=4) would be consistent with a K^+-selective conductance, but no further experiments were conducted to characterize the current and its ion selectivity. Loxapine had no effect on the membrane conductance of non-transfected CHO cells (Figure S1A, B) and was therefore more suitable for these experiments.

Firstly, to replicate the importance of the previously proposed Na^+-sensor, D839 was mutated both to glutamate and alanine. The D839E mutation, which lengthened the sidechain without affecting the negative charge, gave currents that were qualitatively no different to WT $K_{Na}1.1$. The current-voltage relationships closely resembled the WT $K_{Na}1.1$ channel with 10 mM and 40 mM intracellular Na^+, and no currents were recorded in 0 mM intracellular Na^+ (Figure 2B). Consistent with Zhang and others (17), no currents were recorded in the presence of 0, 10 and 40 mM intracellular Na^+ from D839A channels. Large, relatively voltage-independent currents were yielded upon perfusion of 30 μM loxapine into the bath solution, confirming the presence of this Na^+-insensitive mutant $K_{Na}1.1$ channel at the cell membrane (Figure 2).

The conformational change in the βN-αQ loop and D884 controls the activation state of $K_{Na}1.1$ channels

The analysis of protein structures suggested that the movement of the D884 through the rotation of the βN-αQ loop could be a key step in the process of $K_{Na}1.1$ activation by Na^+. Alternatively, through its negative charge, it could be a candidate for Na^+-binding, so we mutated D884 to alanine. Unexpectedly, this resulted in a large increase in channel activity and apparent loss of Na^+-dependence. The voltage-dependent currents recorded from CHO cells expressing D884A $K_{Na}1.1$ with 0, 10 or 40 mM intracellular Na^+ were all similar (Figure 3A and Figure S2A). Perfusion of 30 μM loxapine to cells had little effect on the current amplitude apart from an apparent loss of voltage-dependence, as indicated by a straightening of the current-voltage relationship (Figure 3B). Mutation of the same residue to valine, which has a longer sidechain by just one carbon, had similar effects (Figure 3).

Activation midpoints derived from conductance-voltage relationships fitted with a Boltzmann equation for D884A and D884V in 10 mM Na^+ were significantly hyperpolarized compared to WT $K_{Na}1.1$ (Table 1). With 40 mM intracellular Na^+, the activation midpoints for D884A and D884V $K_{Na}1.1$ were not significantly different from WT $K_{Na}1.1$ under the same conditions. Whilst WT $K_{Na}1.1$ currents were negligible with 0 mM intracellular Na^+, the activation midpoints for D884A and D884V with 0 mM Na^+ were not significantly different to those obtained with 10 and 40 mM Na^+ (Table 1).

Upon increasing the size of the hydrophobic sidechain further by mutating D884 to isoleucine and phenylalanine, different effects were observed. D884I $K_{Na}1.1$ currents were similar to those obtained from WT $K_{Na}1.1$ with each intracellular Na^+ concentration tested (Figure 3B, Figure S2A, Table 1). In contrast, no discernible current could be recorded from D884F $K_{Na}1.1$ with any of the Na^+ concentrations tested up to 40 mM, though function was rescued by loxapine application (Figure 3C). Finally, we mutated D884 to glutamate, which retained the negative charge but increased the sidechain by one carbon. The D884E mutation in $K_{Na}1.1$ had an effect similar to D884F, with negligible currents with each of 0, 10, and 40 mM intracellular Na^+, but large whole-cell currents were recorded following the application of loxapine (Figure 3A, C and Figure S2A).

These results suggested that it could be the size and not the charge of the side chain at amino acid position 884 that determined whether the $K_{Na}1.1$ channel remained Na^+-dependent or became locked in either the inactive or Na^+-activated state under these conditions. We returned to the structure of the Na^+-activated $K_{Na}1.1$ channel and modeled the D884 mutations *in silico*. Whilst aspartate and isoleucine at position 884 could be closely accommodated in the surrounding βO pocket, together with the smaller alanine and valine sidechains with some leeway, substituting the larger glutamate and phenylalanine sidechains resulted in steric clashes with T922 (Figure 4). Additional energy minimization steps with the D884I model did not result in any discernable changes in orientation in involving these sidechains (Figure S3A). D884 was mutated to asparagine in rat $K_{Na}1.1$ by Xu and others (21), resulting in Na^+ -insensitivity, and we found that this mutation could also result in a steric clash *in silico* (Figure S3B).

The role of K885 and residues in or near the βO strand in Na^+-activation

The structural analysis conducted above suggested that Na^+-activation causes the βN-αQ loop to transition from a disordered state to a conformation that could potentially be

stabilized by a salt bridge between D839 (studied above) and K885. To test this idea, K885 was neutralized to alanine. Like with D839A $K_{Na}1.1$, negligible currents were recorded from cells expressing K885A $K_{Na}1.1$ with 0 mM and 10 mM intracellular Na^+ (Figure 5, Figure S2B). A small current was recorded from K885A $K_{Na}1.1$ when intracellular Na^+ was elevated to 40 mM, suggesting a substantial decrease in Na^+-sensitivity of the channel. Functional expression of K885A $K_{Na}1.1$ channels was again confirmed by addition of 30 μM loxapine, which evoked large whole cell currents comparable with those we observed earlier in the study.

We then questioned if the negatively charged (D898 and E920) or polar (T922) sidechains in the vicinity of the pocket accommodating D884 in the activated state played a role in activation by Na^+. Mutation of each of these to alanine similarly disrupted Na^+ activation with no significant currents recorded with 0, 10, or 40 mM intracellular Na^+ (Figure 5, Figure S2B). Functional rescue was achieved with each of these mutant $K_{Na}1.1$ channels following application of 30 μM loxapine. We initially considered whether these residues might contribute to a site for Na^+ to occupy and activate the channel. To see if we could rescue one of these mutations, E920A, or attract D884 into this site and increase activity, D898 and T922 were mutated to the positively charged lysine. However, with each of the D898K, E920A/D898K, and T922K $K_{Na}1.1$ channels the effect was same as the alanine substitutions in this pocket (Figure 5, Figure S2B). Again, no currents were recorded with 0, 10, or 40 mM intracellular Na^+ and functional rescue was achieved with 30 μM loxapine application. We found that that mutation of D898 to either alanine or lysine appeared to result in a weak inward rectification in loxapine-evoked current-voltage relationships (Figure 5B).

Discussion

Our data suggest that the βN-αQ loop in RCK2 of $K_{Na}1.1$ acts as a molecular switch, controlling transitions between the Na^+-activated and Na^+-free inactive states. In the activated state, this loop may be stabilized by a salt bridge between K885 and D839. This explains why previous mutations of this aspartate, D812 in rat $K_{Na}1.1$, by Zhang and others (17) resulted in a loss of Na^+-sensitivity, leading to their proposal that this formed a Na^+-binding site. Concurrently, the ability of D884 to occupy a pocket formed by the βO strand in the activated state appears to be important for activation. Mutating this sidechain to either phenylalanine or glutamate prevented $K_{Na}1.1$ channel activation by 40 mM intracellular Na^+ but mutation to either alanine or valine caused the channel to adopt a constitutively activated, but voltage-gated, Na^+-independent state. This could imply that the conformation

adopted by this pocket in the absence of Na^+ prevents D884 and the βN-αQ loop from adopting the stabilized state, but can accommodate alanine and valine sidechains in place of D884. This domain is highly conserved between $K_{Na}1.1$ and $K_{Na}1.2$, including each of the residues described here (Figure 1A), indicating a common mechanism.

One possible explanation for the different effects of the mutations relates solely to the size of the sidechain at position D884 as considered in the *in silico* mutagenesis (Figure 4). However, the amino acid substitutions may have wider-reaching effects on the protein structure through changes to the electrostatics in the locality of this region. Rather than promoting (D884A, D884V) or preventing (D884F, D884E) the adoption of the Na^+-activated conformation, converse effects of these mutations on the apo state might underlie these effects. Furthermore, given the near 180° rotation of the βN-αQ loop between these two states, the mutations may affect the intervening conformational dynamics.

D884 was recently proposed by both Xu and others (21) and Zhang and others (22) to contribute to a potential cation binding site. Mutating the equivalent of D884 in rat $K_{Na}1.1$ to asparagine rendered the channel non-functional at intracellular Na^+ concentrations to up to 2 M (21). Consequently, and supported by molecular dynamics simulations, this aspartate was proposed as one of two Na^+-binding sites in each subunit. In contrast, we found that the charge of this residue is not critical to $K_{Na}1.1$ channel function, since D884I $K_{Na}1.1$ channels behaved similarly to WT $K_{Na}1.1$. *In silico* mutagenesis of this aspartate in the chicken $K_{Na}1.1$ structure to asparagine caused a steric clash with acidic pocket residues, similar to D884E and D884F, which substitutions prevented Na^+-activation in our experiments. This explains the lack of activity with the asparagine mutation observed by Xu and others (21). D884 is part of cation-binding “site 2” identified by Zhang and others (22), who also studied the D884A $K_{Na}1.1$ mutation. Using intracellular Na^+ concentrations upwards from 100 mM, they found a four-fold decrease in the Na^+ EC_{50}. Since we recorded activated $K_{Na}1.1$ channel currents in the absence of Na^+, the residual Na^+-dependence may arise from an alternative Na^+ binding site with these higher concentrations. The anomalous density in cation “site 2” of human $K_{Na}1.1$ described by Zhang and others (22) was attributed to a K^+ ion, co-ordinated simultaneously by D839 and D884. This protein structure was obtained in Na^+-free and KCl-rich conditions and attributed to the “closed” or inactive conformation. The structure of this region in the activated or “open” human $K_{Na}1.1$ described in the same study is similar to that obtained with the chicken homologue (Figure 1) where D884 is effectively replaced by K885 upon the conformational change in the βN-αQ loop, together with a loss of anomalous density in “Site 2”. The significance of K^+ binding to this site in the inactive conformation is not known, but it is important to note that it is vacated by D884 upon Na^+-activation.

We are unable to propose a specific Na^+-binding site from our investigation, but mutagenesis of residues D898, E920 and T922 that also disrupted Na^+ activation would support the ideas that Na^+ binds in this region. These residues may have a role in co-ordinating Na^+ ions, consistent with E920 having been identified by Xu and others (21) as a Na^+ co-ordinating sidechain, and may underlie the structural change required to accommodate D884 by the βO strand. Mutation of one of these residues, D898, to either lysine or alanine resulted in inward rectification of the $K_{Na}1.1$ current-voltage relationship when activated by loxapine. It was noted in the structure of the chicken $K_{Na}1.1$ channel that the ring of RCK domains forms a "funnel" that narrows as it approaches the pore-forming region and has a largely electronegative surface (19). D898 contributes to this highly negatively charged surface which may contribute to ion conduction. The negatively charged residues are thought to attract K^+ ions and contribute to the relatively high K^+ conductance of this and other member of the channel subfamily, and mutation of D898 may have an effect of outward K^+ currents, leading to the slight inward rectification observed.

Consistent with the model presented here, the rotation and adoption of a stable alpha helix by the βN-αQ loop in RCK2 in the activated, but disordered in the Na^+-free $K_{Na}1.1$ conformation was highlighted in the recently published structure of human $K_{Na}1.1$ (17). The authors argue that this conformational change influences interactions between RCK2 and RCK1 domains, resulting in the overall expansion that opens the channel gate. In conclusion, this structural and our functional data point to this loop as the key regulator of K_{Na} channel activation by Na^+. The constitutive activity with the D884A and D884V mutant $K_{Na}1.1$ in the absence of Na^+ provide further clues to how this channel is regulated. Given that these mutant channels, with the smaller side chain, are able to activate without Na^+, this indicates that the WT channel is primed for activation but requires a small structural change caused by Na^+ binding to enable the βN-αQ loop to adopt the activated state. It is this inactive, but primed state that may be disrupted by inherited mutations that result in $K_{Na}1.1$ gain of function.

Author contributions

BAC, JDL, ACK, and SPM designed the study. BAC and JDL performed research. BAC, JDL, ACK, SPM, and NP analyzed and interpreted data. BAC and JDL drafted the manuscript. BAC, JDL, ACK, SPM, and NP edited and approved the manuscript.

Declaration of Interests

The authors declare no competing interests.

Acknowledgments

Supported by a BBSRC-CASE PhD studentship in conjunction with Autifony Therapeutics Ltd awarded to B.A.C. (BB/M011151/1). For the purpose of open access, the authors have applied a Creative Commons Attribution (CC BY) license to any Author Accepted Manuscript version arising from this submission.

References

1. Yuan, A., C. M. Santi, A. Wei, Z. W. Wang, K. Pollak, M. Nonet, L. Kaczmarek, C. M. Crowder, and L. Salkoff. 2003. The sodium-activated potassium channel is encoded by a member of the Slo gene family. Neuron 37(5):765-773.
2. Hage, T. A., and L. Salkoff. 2012. Sodium-activated potassium channels are functionally coupled to persistent sodium currents. J Neurosci 32(8):2714-2721.
3. Li, P., C. M. Halabi, R. Stewart, A. Butler, B. Brown, X. Xia, C. Santi, S. England, J. Ferreira, R. P. Mecham, and L. Salkoff. 2019. Sodium-activated potassium channels moderate excitability in vascular smooth muscle. J Physiol 597(20):5093-5108.
4. Nanou, E., A. Kyriakatos, A. Bhattacharjee, L. K. Kaczmarek, G. Paratcha, and A. El Manira. 2008. Na+-mediated coupling between AMPA receptors and KNa channels shapes synaptic transmission. Proc Natl Acad Sci U S A 105(52):20941-20946.
5. Kessi, M., B. Chen, J. Peng, Y. Tang, E. Olatoutou, F. He, L. Yang, and F. Yin. 2020. Intellectual Disability and Potassium Channelopathies: A Systematic Review. Frontiers in Genetics 11:614.
6. Bonardi, C. M., H. O. Heyne, M. Fiannacca, M. P. Fitzgerald, E. Gardella, B. Gunning, K. Olofsson, G. Lesca, N. Verbeek, H. Stamberger, P. Striano, F. Zara, M. M. Mancardi, C. Nava, S. Syrbe, S. Buono, S. Baulac, A. Coppola, S. Weckhuysen, A. S. Schoonjans, B. Ceulemans, C. Sarret, T. Baumgartner, H. Muhle, V. D. Portes, J. Toulouse, M. C. Nougues, M. Rossi, G. Demarquay, D. Ville, E. Hirsch, H. Maurey, M. Willems, J. de Bellescize, C. D. Altuzarra, N. Villeneuve, F. Bartolomei, F. Picard,

F. Hornemann, D. A. Koolen, H. Y. Kroes, C. Reale, C. D. Fenger, W. H. Tan, L. Dibbens, D. R. Bearden, R. S. Møller, and G. Rubboli. 2021. KCNT1-related epilepsies and epileptic encephalopathies: phenotypic and mutational spectrum. Brain 144(12):3635-3650.

7. Barcia, G., M. R. Fleming, A. Deligniere, V. R. Gazula, M. R. Brown, M. Langouet, H. Chen, J. Kronengold, A. Abhyankar, R. Cilio, P. Nitschke, A. Kaminska, N. Boddaert, J. L. Casanova, I. Desguerre, A. Munnich, O. Dulac, L. K. Kaczmarek, L. Colleaux, and R. Nabbout. 2012. De novo gain-of-function KCNT1 channel mutations cause malignant migrating partial seizures of infancy. Nat Genet 44(11):1255-1259.
8. Heron, S. E., K. R. Smith, M. Bahlo, L. Nobili, E. Kahana, L. Licchetta, K. L. Oliver, A. Mazarib, Z. Afawi, A. Korczyn, G. Plazzi, S. Petrou, S. F. Berkovic, I. E. Scheffer, and L. M. Dibbens. 2012. Missense mutations in the sodium-gated potassium channel gene KCNT1 cause severe autosomal dominant nocturnal frontal lobe epilepsy. Nat Genet 44(11):1188-1190.
9. Mao, X., N. Bruneau, Q. Gao, H. Becq, Z. Jia, H. Xi, L. Shu, H. Wang, P. Szepetowski, and L. Aniksztejn. 2020. The Epilepsy of Infancy With Migrating Focal Seizures: Identification of de novo Mutations of the KCNT2 Gene That Exert Inhibitory Effects on the Corresponding Heteromeric K(Na)1.1/K(Na)1.2 Potassium Channel. Front Cell Neurosci 14:1.
10. Cioclu, M. C., I. Mosca, P. Ambrosino, D. Puzo, A. Bayat, S. B. Wortmann, J. Koch, V. Strehlow, K. Shirai, N. Matsumoto, S. J. Sanders, V. Michaud, M. Legendre, A. Riva, P. Striano, H. Muhle, M. Pendziwiat, G. Lesca, G. D. Mangano, R. Nardello, J. R. Lemke, R. S. Møller, M. V. Soldovieri, G. Rubboli, and M. Taglialatela. 2023. KCNT2-Related Disorders: Phenotypes, Functional, and Pharmacological Properties. Ann Neurol 94(2):332-349.
11. Yang, B., V. K. Gribkoff, J. Pan, V. Damagnez, S. I. Dworetzky, C. G. Boissard, A. Bhattacharjee, Y. Yan, F. J. Sigworth, and L. K. Kaczmarek. 2006. Pharmacological activation and inhibition of Slack (Slo2.2) channels. Neuropharmacology 51(4):896-906.
12. de Los Angeles Tejada, M., K. Stolpe, A. K. Meinild, and D. A. Klaerke. 2012. Clofilium inhibits Slick and Slack potassium channels. Biologics 6:465-470.
13. Biton, B., S. Sethuramanujam, K. E. Picchione, A. Bhattacharjee, N. Khessibi, F. Chesney, C. Lanneau, O. Curet, and P. Avenet. 2012. The antipsychotic drug loxapine is an opener of the sodium-activated potassium channel slack (Slo2.2). J Pharmacol Exp Ther 340(3):706-715.
14. Cole, B. A., R. M. Johnson, H. Dejakaisaya, N. Pilati, C. W. G. Fishwick, S. P. Muench, and J. D. Lippiat. 2020. Structure-Based Identification and Characterization

of Inhibitors of the Epilepsy-Associated KNa1.1 (KCNT1) Potassium Channel. iScience 23(5):101100.

15. Spitznagel, B. D., N. M. Mishra, A. M. Qunies, F. J. Prael, 3rd, Y. Du, K. A. Kozek, R. M. Lazarenko, J. S. Denton, K. A. Emmitte, and C. D. Weaver. 2020. VU0606170, a Selective Slack Channels Inhibitor, Decreases Calcium Oscillations in Cultured Cortical Neurons. ACS Chem Neurosci 11(21):3658-3671.
16. Griffin, A. M., K. M. Kahlig, R. J. Hatch, Z. A. Hughes, M. L. Chapman, B. Antonio, B. E. Marron, M. Wittmann, and G. Martinez-Botella. 2021. Discovery of the First Orally Available, Selective KNa1.1 Inhibitor: In Vitro and In Vivo Activity of an Oxadiazole Series. ACS Medicinal Chemistry Letters 12(4):593-602.
17. Zhang, Z., A. Rosenhouse-Dantsker, Q. Y. Tang, S. Noskov, and D. E. Logothetis. 2010. The RCK2 domain uses a coordination site present in Kir channels to confer sodium sensitivity to Slo2.2 channels. J Neurosci 30(22):7554-7562.
18. Thomson, S. J., A. Hansen, and M. C. Sanguinetti. 2015. Identification of the Intracellular Na+ Sensor in Slo2.1 Potassium Channels. J Biol Chem 290(23):14528-14535.
19. Hite, R. K., P. Yuan, Z. Li, Y. Hsuing, T. Walz, and R. MacKinnon. 2015. Cryo-electron microscopy structure of the Slo2.2 Na(+)-activated K(+) channel. Nature 527(7577):198-203.
20. Hite, R. K., and R. MacKinnon. 2017. Structural Titration of Slo2.2, a Na+-Dependent K+ Channel. Cell 168(3):390-399.e311.
21. Xu, J., Y.-T. Lv, X.-Y. Zhao, J.-J. Wang, Z.-S. Shen, J. Li, F.-F. Zhang, J. Liu, X.-H. Wang, Y. Xu, Q. Geng, Y.-T. Ding, J.-J. Xu, M.-J. Tan, Z.-X. Li, R. Wang, J. Chen, W. Sun, M. Cui, D. E. Logothetis, J.-l. Cao, Q.-Y. Tang, and Z. Zhang. 2023. Identification of Sodium- and Chloride-Sensitive Sites in the Slack Channel. J Neurosci 43(15):2665-2681.
22. Zhang, J., S. Liu, J. Fan, R. Yan, B. Huang, F. Zhou, T. Yuan, J. Gong, Z. Huang, and D. Jiang. 2023. Structural basis of human Slo2.2 channel gating and modulation. Cell Reports 42(8):112858.
23. Pettersen, E. F., T. D. Goddard, C. C. Huang, G. S. Couch, D. M. Greenblatt, E. C. Meng, and T. E. Ferrin. 2004. UCSF Chimera--a visualization system for exploratory research and analysis. Journal of Computational Chemistry 25(13):1605-1612.
24. Sanner, M. F., A. J. Olson, and J. C. Spehner. 1996. Reduced surface: an efficient way to compute molecular surfaces. Biopolymers 38(3):305-320.
25. Gamper, N., J. D. Stockand, and M. S. Shapiro. 2005. The use of Chinese hamster ovary (CHO) cells in the study of ion channels. J Pharmacol Toxicol Methods 51(3):177-185.

Tables

Table 1: Parameters derived from Boltzmann fit of WT and D884 mutant $K_{Na}1.1$ channel conductance with 0, 10, and 40 mM intracellular Na^+. Data are presented as mean ± SEM (n=5 to 9 cells). $V_{0.5}$ is the half-maximal activation voltage, $^{**}p<0.005$, $^{***}p<0.0005$ compared to WT $V_{0.5}$ with 10 mM intracellular Na^+ (independent one-way ANOVA with Tukey's post-hoc test). *z* was derived from the slope of the Boltzmann curve, *RT*/*zF*. No significant differences in *z* were found with mutant $K_{Na}1.1$ compared to wild-type with either 10 or 40 mM intracellular Na^+ (ANOVA),

$K_{Na}1.1$ variant	$[Na^+]_i$	$V_{0.5}$ (mV)	*z*
WT	**10 mM**	2.15 ± 3.69	0.81 ± 0.09
	40 mM	-46.63 ± 8.06	0.75 ± 0.14
D884A	**0 mM**	-60.28 ± 9.60	0.47 ± 0.03
	10 mM	-61.92 ± 6.77***	0.60 ± 0.07
	40 mM	-60.33 ± 8.36	0.59 ± 0.09
D884V	**0 mM**	-46.99 ± 11.08	0.61 ± 0.07
	10 mM	-61.08 ± 3.23**	0.57 ± 0.04
	40 mM	-60.86 ± 4.89	0.57 ± 0.08
D884I	**10 mM**	0.23 ± 6.78	0.92 ± 0.02
	40 mM	-39.17 ± 14.32	0.66 ± 0.09

Figure Legends

Figure 1 Structural analysis of the Na^+-binding site proposed by Zhang and others (17) in chicken $K_{Na}1.1$ channel protein resolved using cryo-EM. **A** Structure of chicken $K_{Na}1.1$ in the active conformation (PDB: 5U70) with one subunit in the tetramer colored blue. Each subunit comprises 6 transmembrane helices (upper part of structure), and a re-entrant P-loop between S5 and S6 that forms the K^+-selective filter. The large intracellular domains contain a pair of RCK domains, RCK1 and RCK2 (lower part of structure). The domain of interest in RCK2 is enclosed by the black box. **B** Enlarged representation of the domain of interest with the active (blue) and inactive (PDB:5U76, dark gray) conformations overlaid. The aspartate identified by Zhang and others (17) is D839 (all human $K_{Na}1.1$ numbering).

The twisting of a nearby loop between βN-αQ in RCK2, indicated by the green arrows, with a lysine (K885) close enough to form a salt bridge with the purported Na^+-binding aspartate (D839) in the Na^+-activated state. Concurrently, an aspartate (D884) in the same loop adopts a position proximal to the βO strand and flanked by E920 and T922. The βN-αQ loop is not resolved in the inactive state (dashed line), indicating disorder. **C** Sequence alignment of the domain of interest between $K_{Na}1.1$ from human (h), chicken (c), and rat (r), plus the closely-related human $K_{Na}1.2$. Conserved residues (with respect to $hK_{Na}1.1$) are shaded green. The domain structure (22) is shown by the blue shapes and the amino acids labelled in panel B are indicated by asterisks.

Figure 2 Mutational analysis of the previously proposed Na^+ sensor. A Representative whole cell currents from CHO cells transfected with WT or mutant human $K_{Na}1.1$, with intracellular Na^+ and drug exposure as indicated, in response to 400 ms steps from -100 to +80 mV in 10 mV increments from a holding potential of -80 mV. The dashed lines indicate the zero-current level. **B** Mean (± SEM, n=5 to 8 cells) current-voltage relationships for WT and mutant $K_{Na}1.1$ channels in the presence of 0 (red ●), 10 (black ■) and 40 (green ♦ or ▲) mM intracellular Na^+, or 10 mM Na^+ and 30 μM loxapine (dark blue ▼). **C** Mean bar with SEM and individual data points for current density at +10 mV from the data presented in panel **B**, with the same color representation.

Figure 3 Role of D884 in controlling $K_{Na}1.1$ channel activation. A Representative D884A, D884I, and D884E $K_{Na}1.1$ whole cell currents in response to 400 ms steps from -100 to +80 mV in 10 mV increments, from a holding potential of -80 mV. The dashed lines indicate the zero-current level. **B** Mean ± SEM (n=5 to 8 cells) current-voltage and conductance-voltage relationships for D884A, D884V, and D884I $K_{Na}1.1$ with 0 (red ●), 10 (black ■) and 40 (green ◆) mM intracellular Na^+, or 10 mM Na^+ and 30 μM loxapine (dark blue ▼). The mean conductance-voltage relationship for WT $K_{Na}1.1$ recorded with 10 mM intracellular Na^+ is indicated by a dotted line for comparison. **C** Mean ± SEM current-voltage relationships for D884F and D884E $K_{Na}1.1$ with 0 (red ●), 10 (black ■) and 40 (green ▲) mM intracellular Na^+, or 10 mM Na^+ and 30 μM loxapine (dark blue ▼).

Figure 4 Molecular modelling of D884 mutations. Models were generated from the structure of chicken $K_{Na}1.1$ in the Na^+-activated state (PDB: 5U70), here with the numbering of conserved residues in human $K_{Na}1.1$. In each model the pocket formed by ^{920}ELT^{922} in the βO strand is shown with pale gray space fill, with ^{882}VVDKE^{886} in the βN-αQ loop with pale gold space fill below. With the D884F and D884E substitutions, predicted atomic clashes between the substituted sidechains and T922 are indicated by solid black lines. No clashes were predicted in the other models.

Figure 5 Disruption of Na^+ activation through loss of a potential D839/K885 salt bridge and residues in or near βO. A Representative whole cell K885A and D898K $K_{Na}1.1$ currents in each condition, as indicated, in response to 400 ms steps from -100 to +80 mV in 10 mV increments, from a holding potential of -80 mV. The dashed lines indicate the zero-current level. **B** Mean (± SEM, n=5 to 8 cells) current-voltage relationships for mutated $K_{Na}1.1$ channels in the presence of 0 (red ●), 10 (black ■) and 40 (green ▲) mM intracellular Na^+, or 10 mM Na^+ and 30 μM loxapine (dark blue ▼).

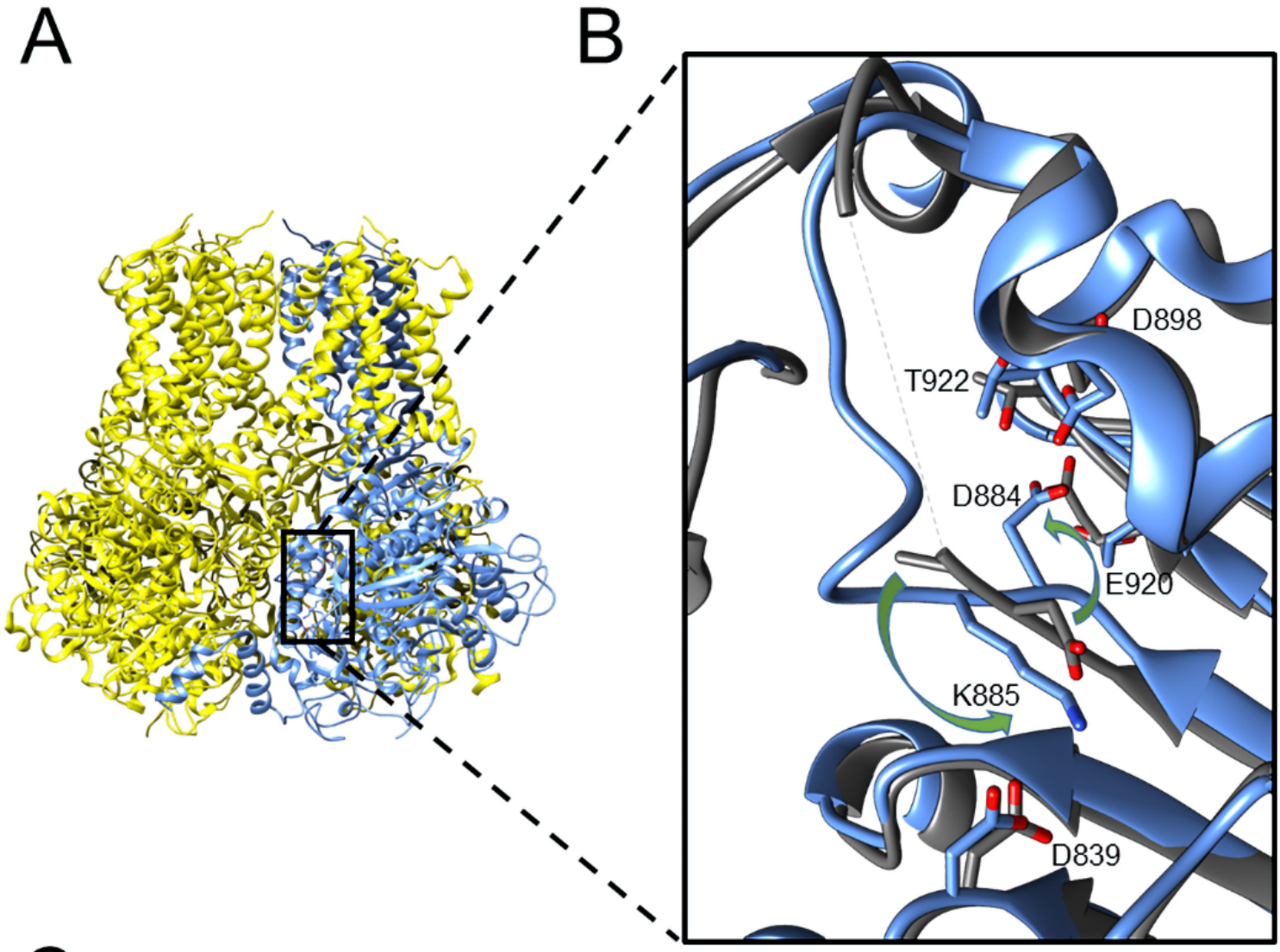

C

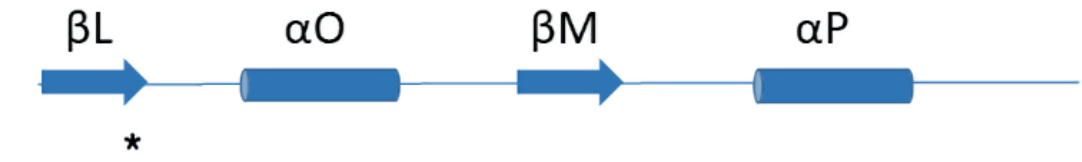


```
                *
hKNa1.1   835 VLLLDNKPDHHFLEAICCFPMVYYMEGSVDNLDSLLQCGIIYADN 879
cKNa1.1   808 VLLLDNKPEHHFLEAICCFPMVYYMEGTIDNLDSLLQCGIIYADN 852
rKNa1.1   814 VLLLDNKPDHHFLEAICCFPMVYYMEGSVDNLDSLLQCGIIYADN 858
hKNa1.2   753 VLLLDNPPDMHFLDAICWFPMVYYMVGSIDNLDDLLRCGVTFAAN 797
```

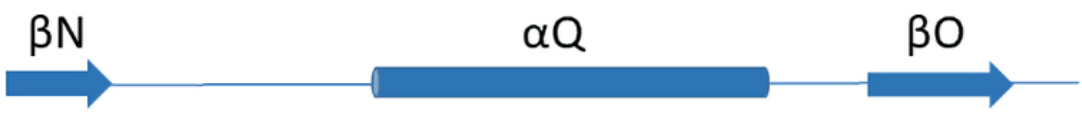


```
                **          *            * *
hKNa1.1   880 LVVVDKESTMSAEEDYMADAKTIVNVQTMFRLFPSLSITTELTHP 924
cKNa1.1   853 LVVVDKESTMSAEEDYMADAKTIVNVQTMFRLFPSLSITELTHP 897
rKNa1.1   859 LVVVDKESTMSAEEDYMADAKTIVNVQTMFRLFPSLSITTELTHP 903
hKNa1.2   798 MVVVDKESTMSAEEDYMADAKTIVNVQTLFRLFSSLSITELTHP 842
```

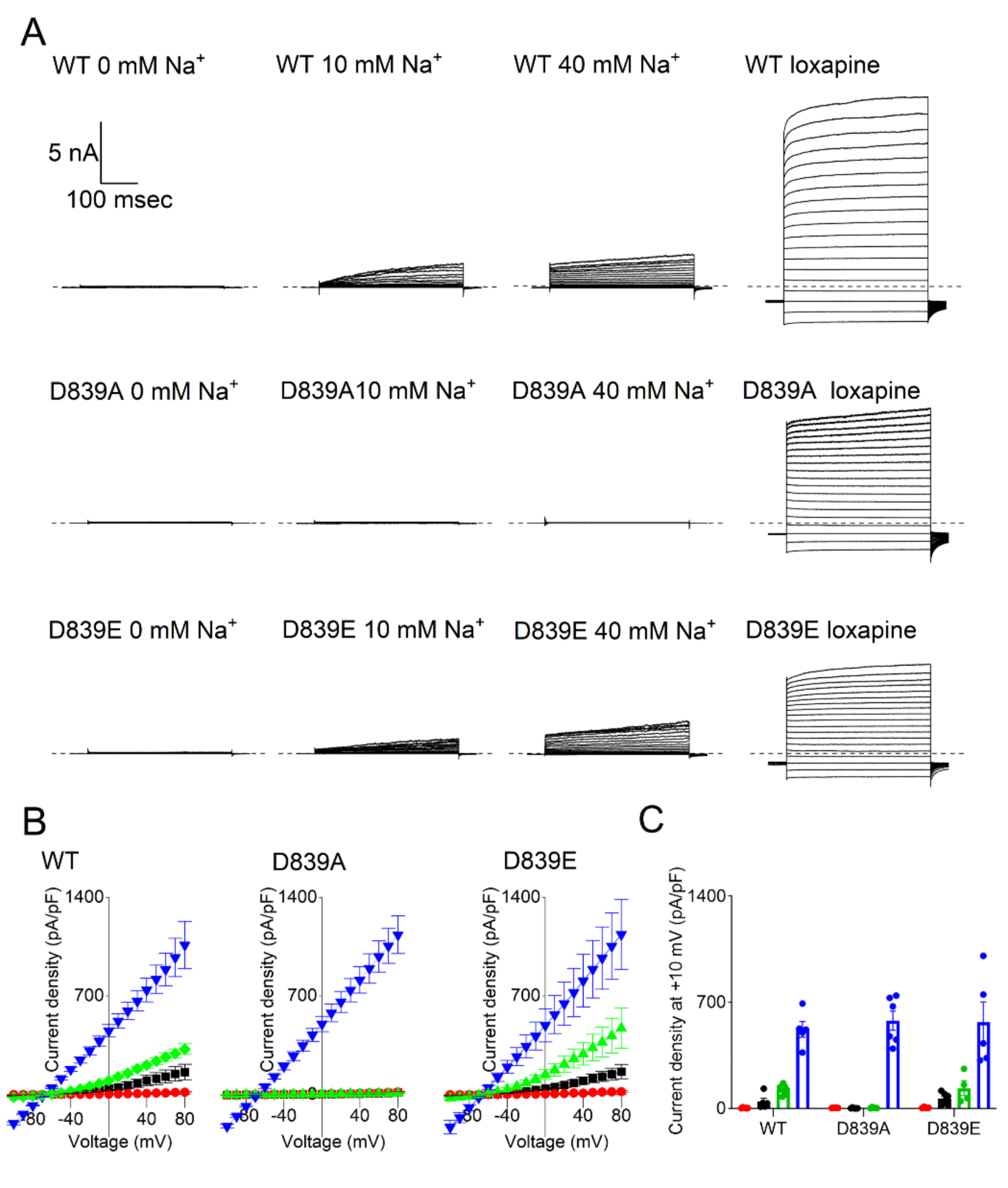
A
WT 0 mM Na+
WT 10 mM Na+
WT 40 mM Na+
WT loxapine
5 nA
100 msec
D839A 0 mM Na+
D839A10 mM Na+
D839A 40 mM Na+
D839A loxapine
D839E 0 mM Na+
D839E 10 mM Na+
D839E 40 mM Na+
D839E loxapine
B
WT
D839A
D839E
Current density (pA/pF)
1400
700
0
-80
-40
40
80
Voltage (mV)
C
Current density at +10 mV (pA/pF)
1400
700
0
WT
D839A
D839E

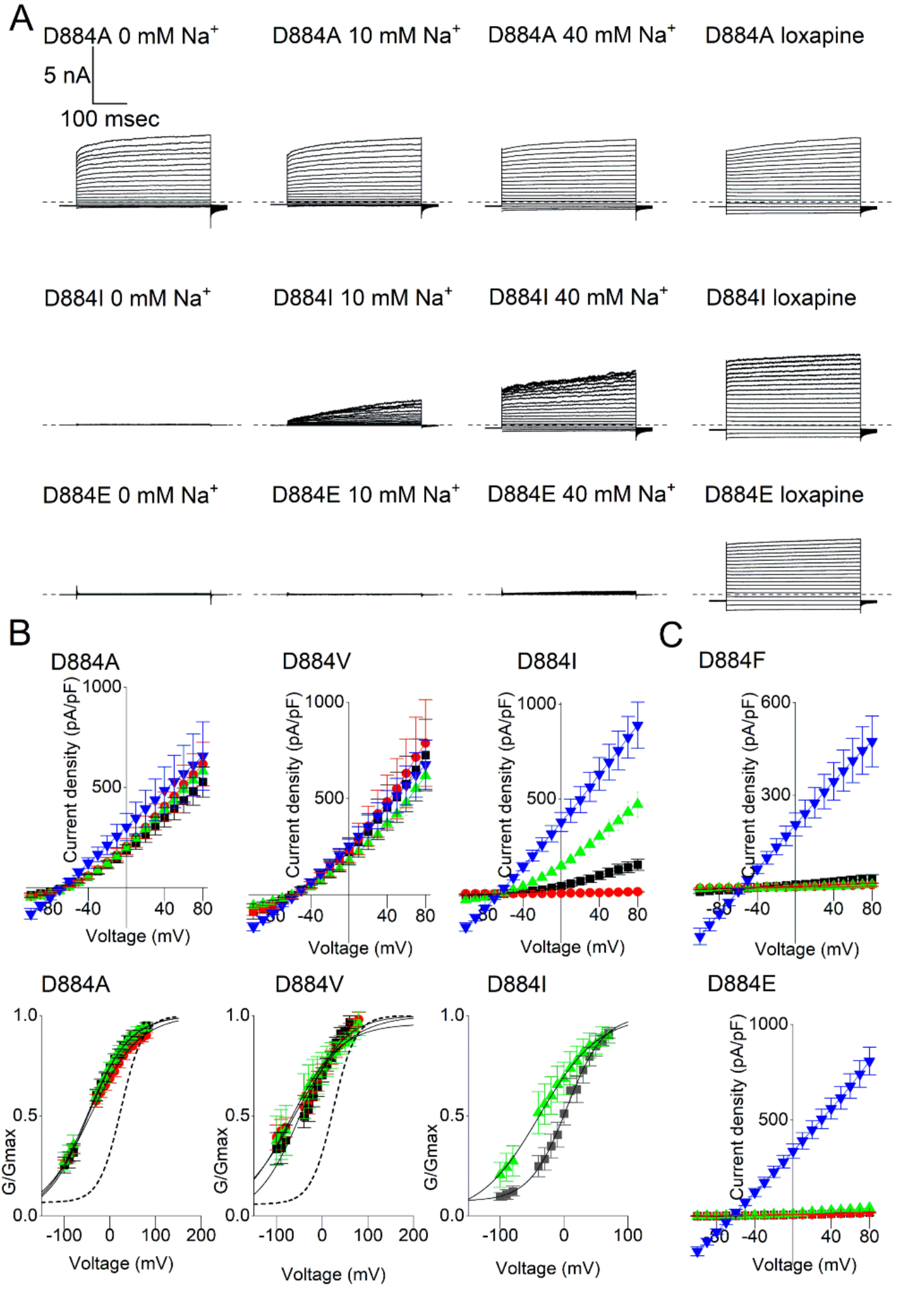
A
D884A 0 mM Na+
D884A 10 mM Na+
D884A 40 mM Na+
D884A loxapine
5 nA
100 msec
D884I 0 mM Na+
D884I 10 mM Na+
D884I 40 mM Na+
D884I loxapine
D884E 0 mM Na+
D884E 10 mM Na+
D884E 40 mM Na+
D884E loxapine
B
D884A
D884V
D884I
C
D884F
Current density (pA/pF)
Voltage (mV)
D884A
D884V
D884I
D884E
G/Gmax
Voltage (mV)
Current density (pA/pF)
Voltage (mV)

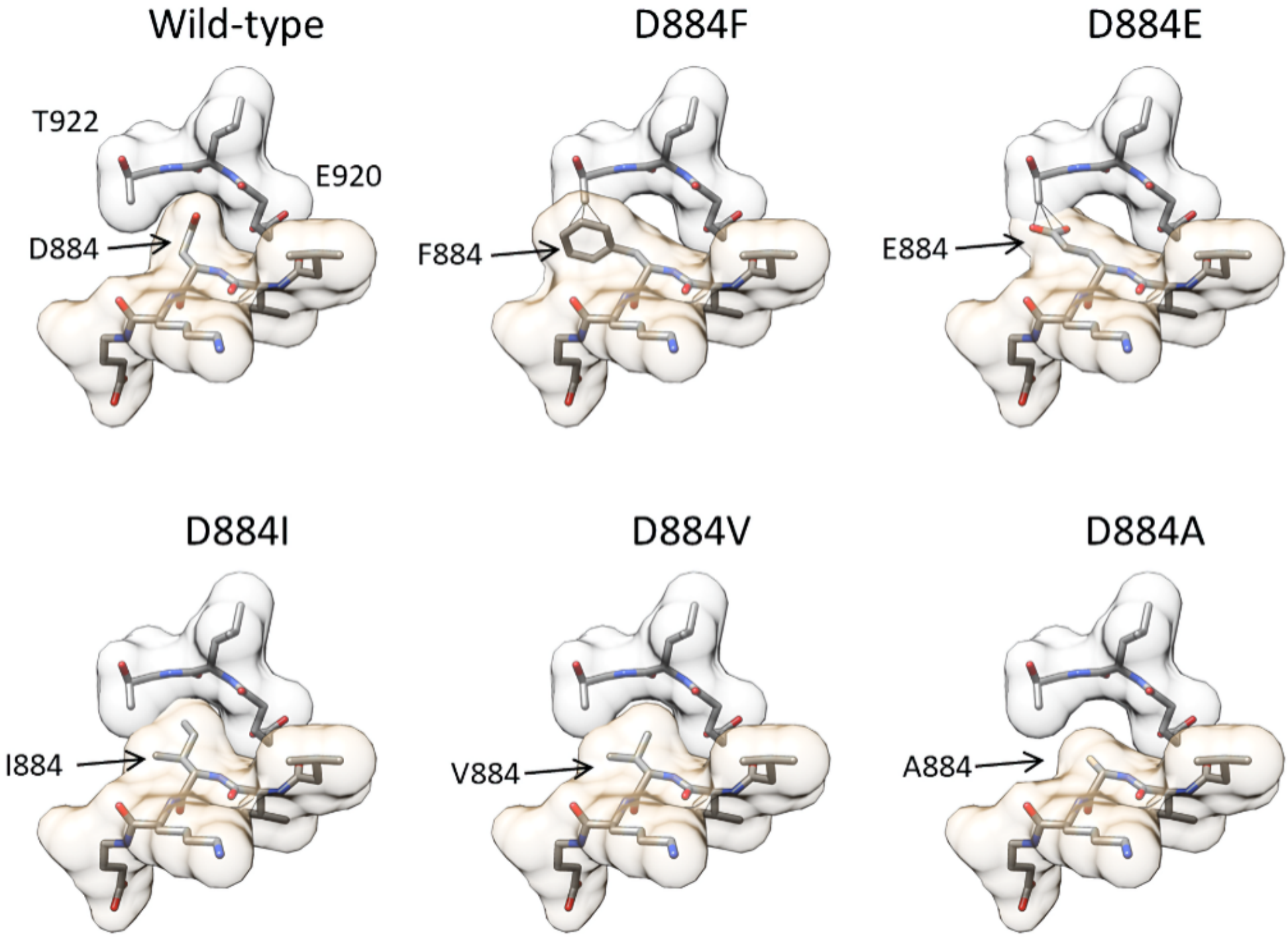
Wild-type
T922
E920
D884
D884F
F884
D884E
E884
D884I
I884
D884V
V884
D884A
A884

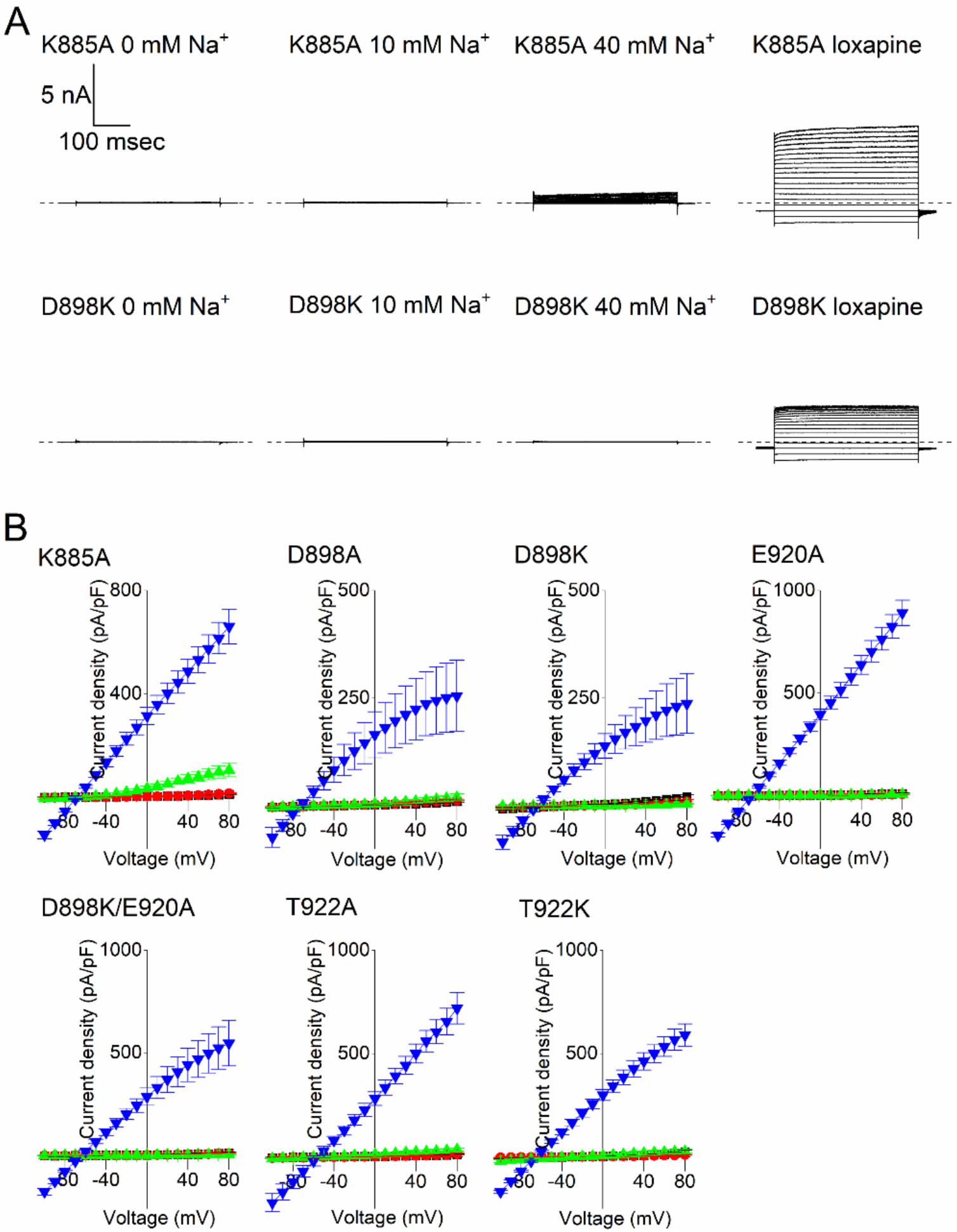
A
K885A 0 mM Na+
K885A 10 mM Na+
K885A 40 mM Na+
K885A loxapine
5 nA
100 msec
D898K 0 mM Na+
D898K 10 mM Na+
D898K 40 mM Na+
D898K loxapine
B
K885A
D898A
D898K
E920A
D898K/E920A
T922A
T922K
Current density (pA/pF)
Voltage (mV)
800
400
500
250
1000
-80
-40
40
80

A molecular switch in RCK2 triggers sodium-dependent activation of K_{Na}1.1 (KCNT1) potassium channels

Bethan A. Cole,[1,5] Antreas C. Kalli,[2,3] Nadia Pilati,[4] Stephen P. Muench,[1,3] and Jonathan D. Lippiat[1]

[1]School of Biomedical Sciences, University of Leeds, Leeds LS2 9JT, UK.

[2]Leeds Institute of Cardiovascular and Metabolic Medicine, University of Leeds, Leeds LS2 9JT, UK.

[3]Astbury Centre for Structural and Molecular Biology, University of Leeds, Leeds LS2 9JT, UK.

[4]Autifony Srl, Padova, 35127, Italy.

[5]Present address: Nuffield Department of Clinical Neurosciences, University of Oxford, Oxford OX3 9DU, UK.

SUPPORTING MATERIAL

Table S1 Equivalent amino acid positions in K_{Na}1.1 channel subunits from the human clone used for electrophysiological experiments in this study and in cryo-EM (1), cryo-EM structures of chicken K_{Na}1.1 (2), and rat K_{Na}1.1 used in previous studies of Na^+-activation of K_{Na}1.1 (3, 4).

Human	Chicken	Rat
E392	E371	E373
D839	D812	D818
D884	D857	D863
K885	K858	K864
D898	D871	D877
E920	E893	E899
T922	T895	T901

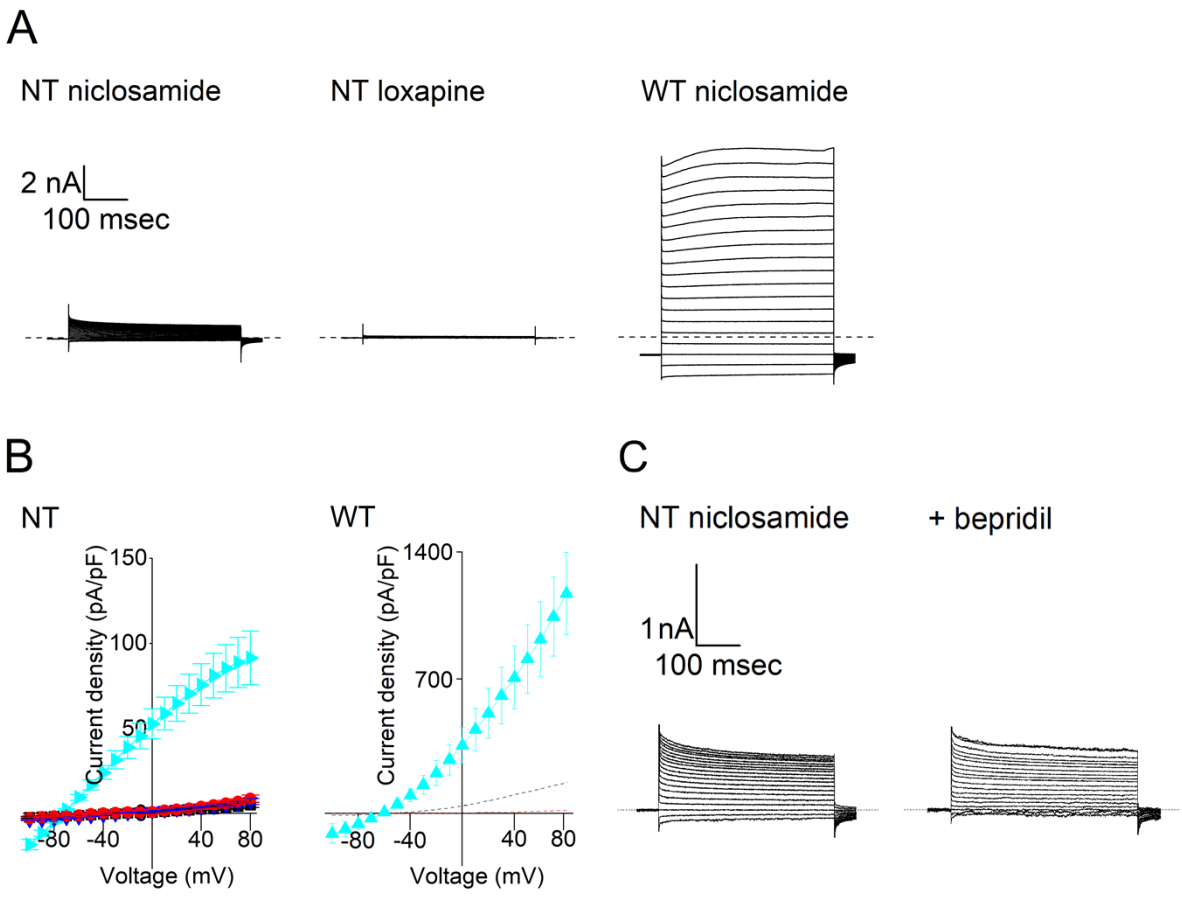

Figure S1. Evaluation of $K_{Na}1.1$ channel activators on control CHO cells. **A** Representative whole cell currents from non-transfected CHO cells (NT) and CHO cells transfected with WT human $K_{Na}1.1$ (WT), as indicated, in response to 400 ms steps from -100 to +80 mV in 10 mV increments from a holding potential of -80 mV. **B** Mean (± SEM, n=5 to 8 cells) current-voltage relationships for NT control in the presence of 0 (red ●), 10 (black ■) mM intracellular Na^+, 10 mM Na^+ + 30 µM niclosamide (cyan ▶) and 10 mM Na^+ + 30 µM loxapine (dark blue ▼), and WT $K_{Na}1.1$ channels in the presence of 30 µM niclosamide (cyan ▶) and 10 mM Na^+. WT $K_{Na}1.1$ current recorded with 10 mM intracellular Na^+ is indicated by a black dotted line, and 0 mM intracellular Na^+ is indicated by a red dotted line. **C** Representative niclosamide-activated whole cell currents from non-transfected CHO cells (NT) in response to 400 ms steps from -100 to +80 mV in 10 mV increments from a holding potential of -80 mV, before (left) and after (right) application of 10 µM bepridil.

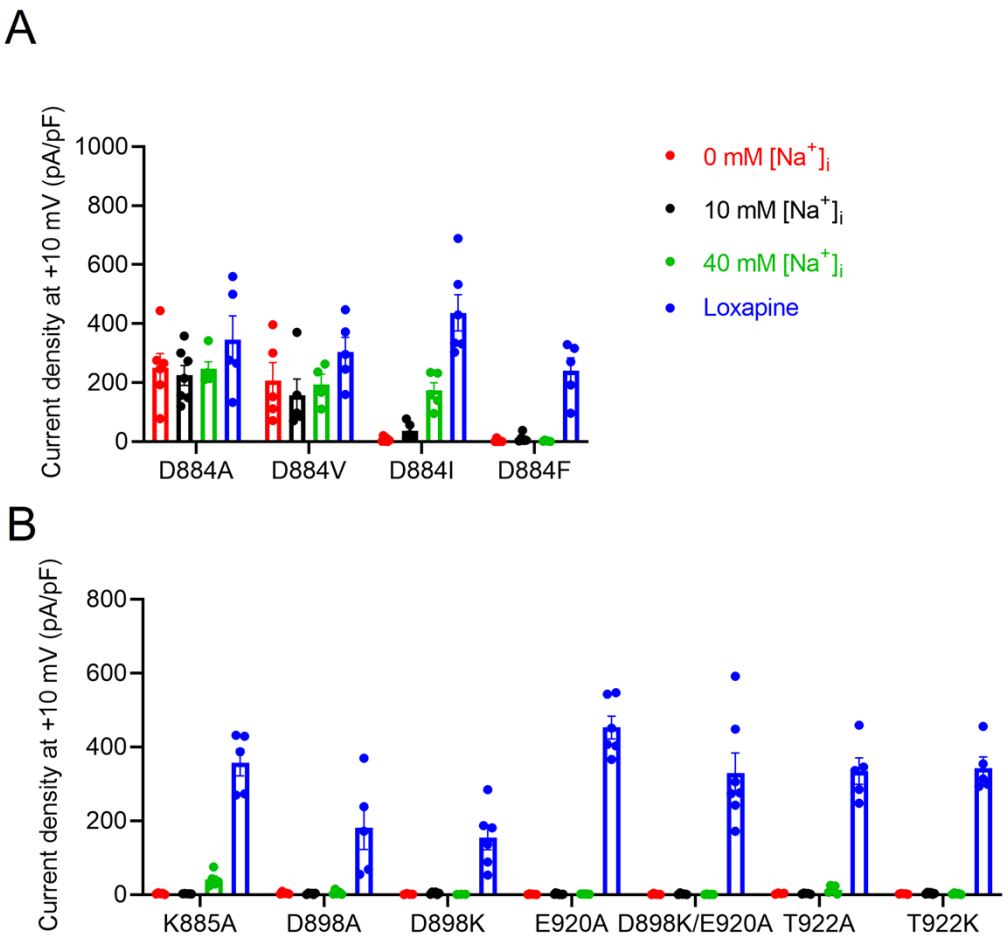

Figure S2. **Distribution of current densities obtained with mutant $K_{Na}1.1$.** Mean bar with SEM and individual data points representing current densities recorded at +10 mV for the mutant $K_{Na}1.1$ presented in main Figure 3 (**A**), and main Figure 5 (**B**).

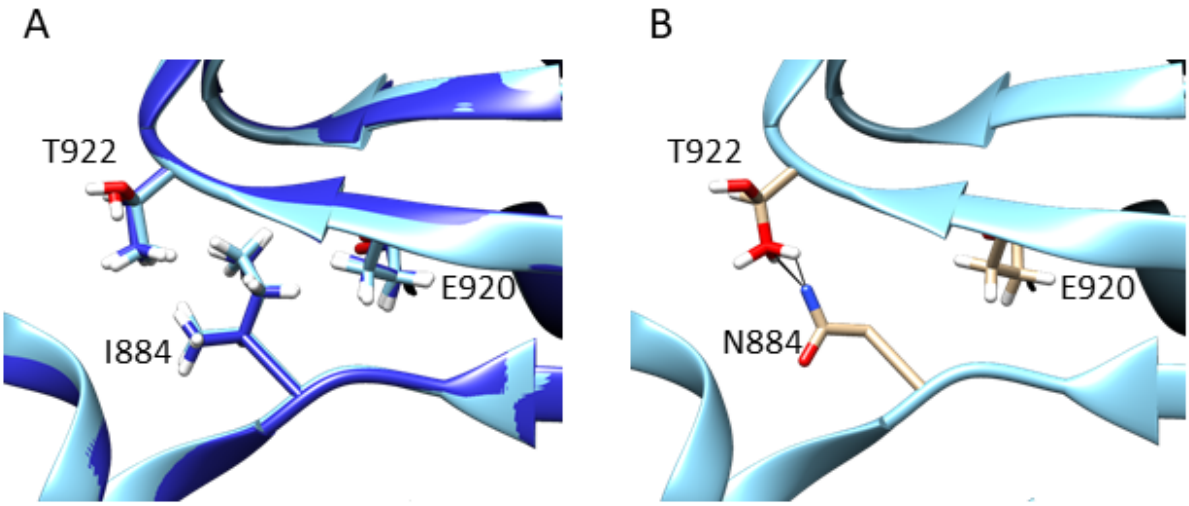

Figure S3. Further in silico modeling of $K_{Na}1.1$ D884. A Substitution of D884 at the equivalent position in activated chicken $K_{Na}1.1$ (PDB: 5U70) with isoleucine before (light blue) and after (dark blue) energy minimization in UCSF Chimera v1.13 (function "Minimize Structure" was used, using default step settings and no fixed atoms). **B** Substitution of D884 in the same model with asparagine (N884). Atomic clashes with T922 are shown by the black lines.

SUPPORTING REFERENCES

1. Zhang, J., S. Liu, J. Fan, R. Yan, B. Huang, F. Zhou, T. Yuan, J. Gong, Z. Huang, and D. Jiang. 2023. Structural basis of human Slo2.2 channel gating and modulation. Cell Reports 42, 112858.
2. Hite, R. K., and R. MacKinnon. 2017. Structural Titration of Slo2.2, a Na(+)-Dependent K(+) Channel. Cell 168, 390-399 e311.
3. Zhang, Z., A. Rosenhouse-Dantsker, Q. Y. Tang, S. Noskov, and D. E. Logothetis. 2010. The RCK2 domain uses a coordination site present in Kir channels to confer sodium sensitivity to Slo2.2 channels. J Neurosci 30, 7554-7562.
4. Xu, J., Y.-T. Lv, X.-Y. Zhao, J.-J. Wang, Z.-S. Shen, J. Li, F.-F. Zhang, J. Liu, X.-H. Wang, Y. Xu, Q. Geng, Y.-T. Ding, J.-J. Xu, M.-J. Tan, Z.-X. Li, R. Wang, J. Chen, W. Sun, M. Cui, D. E. Logothetis, J.-l. Cao, Q.-Y. Tang, and Z. Zhang. 2023. Identification of Sodium- and Chloride-Sensitive Sites in the Slack Channel. J Neurosi 43, 2665-2681.